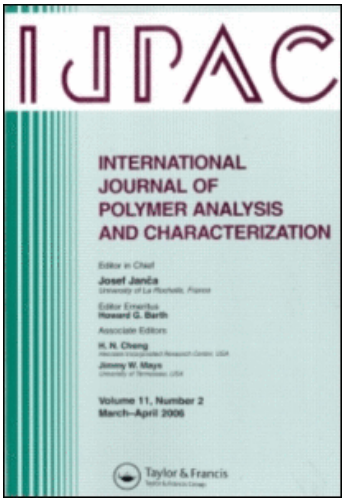

International Journal of Polymer Analysis and Characterization
Publication details, including instructions for authors and subscription information:
http://www.informaworld.com/smpp/title~content=t713646643

A Rheo-Optical FTIR Spectrometer for Investigating Molecular Orientation and Viscoelastic Behavior in Polymers

Gerald R. Hofmann[a]; Michael S. Sevegney[a]; Rangaramanujam M. Kannan[a]
[a] Department of Chemical Engineering and Materials Science, Wayne State University, Detroit, Michigan, USA

To cite this Article Hofmann, Gerald R. , Sevegney, Michael S. and Kannan, Rangaramanujam M.(2004) 'A Rheo-Optical FTIR Spectrometer for Investigating Molecular Orientation and Viscoelastic Behavior in Polymers', International Journal of Polymer Analysis and Characterization, 9: 4, 245 — 274
To link to this Article: DOI: 10.1080/10236660490920237
URL: http://dx.doi.org/10.1080/10236660490920237

International Journal of Polymer Anal. Charact., 9: 245–274, 2004

ISSN: 1023-666X print
DOI:10.1080/10236660490920237

Taylor & Francis
Taylor & Francis Group

A Rheo-Optical FTIR Spectrometer for Investigating Molecular Orientation and Viscoelastic Behavior in Polymers

Gerald R. Hofmann, Michael S. Sevegney, and Rangaramanujam M. Kannan
Department of Chemical Engineering and Materials Science, Wayne State University, Detroit, Michigan, USA

A rheo-optical Fourier transform infrared (FTIR) spectrometer has been developed by combining step-scan FTIR spectroscopy with elements of polarimetry and rheometry in order to investigate both deformation-induced morphology changes and orientation/relaxation dynamics of components within complex polymers. This versatile instrument can directly and sensitively measure quantitative infrared spectra at different temperatures and for different deformation modes. A complex, multiple-modulation/demodulation processing scheme is used to extract both absorbance and dichroism information from a single detector signal. Experimental results from a semicrystalline isotactic polypropylene and a thermoplastic polyurethane are reported in order to illustrate instrument capabilities.

Received 10 December 2003; accepted 22 November 2004.

The authors wish to express their gratitude to Dr. David Drapcho of Bio-Rad Laboratories and Dr. Christopher Manning of Manning Applied Technologies for numerous helpful discussions and assistance with the optimization of the spectrometer, polarimetry, and rheometric hardware. The authors also thank Mr. Gautam Parthasarthy at Wayne State University for his assistance with preparing sample films. This study was supported financially by the Wayne State University Institute of Manufacturing Research (GRH), the Wayne State University Thomas C. Rumble Fellowship (MSS), and the National Science Foundation CAREER Award (DMR9876221) (RMK).

Address correspondence to Rangaramanujam M. Kannan, Department of Chemical Engineering and Materials Science, Wayne State University, 1121 Engineering, 5050 Anthony Wayne Dri., Detroit, MI 48202-3902, USA. E-mail: rkannan@che.eng.wayne.edu

Keywords: Rheo-optics; FTIR spectroscopy; Polymer structure-property relationships

INTRODUCTION

Establishing the relationships between molecular structure and macromechanical (bulk) properties in polymers is an important task in the field of materials science and engineering. Such an understanding is becoming even more critical with emerging synthesis and processing technologies, where property manipulation at microscopic, and even nanoscopic, length scales is desired. Our recent efforts focus on understanding the dynamic behavior of individual chemical functionalities and microstructures within complex polymers as they undergo important processing steps. Specifically, we are studying both changes in morphology (over a range of length scales) and molecular orientation/relaxation responses that are induced by a mechanical perturbation of the bulk material. For example, the morphology of a semicrystalline polymer depends on stereochemical regularity, thermal history, and mechanical processing history[1,2]. Consequently, chemically identical polymers can possess different microstructures (e.g., crystalline, amorphous, mesophase), each responding quite differently to macroscopic deformation.

Optical methods such as birefringence[3–6], X-ray scattering[7–12], and vibrational spectroscopy[13–17] have been used to characterize morphology and molecular orientation in polymers. Each aforementioned technique presents some subtle experimental limitation(s) that can be overcome using rheo-optical Fourier transform infrared (FTIR) spectroscopy. Rheo-FTIR involves the quantitative measurement of anisotropic absorbance (i.e., dichroism) spectra in order to investigate the local polymer physics responsible for macroscopic viscoelastic behavior. Absorption of infrared radiation is sensitive to individual moieties within polymers and thus serves as a good vibrational probe. Linear dichroism—the anisotropic absorption by a material of two mutually perpendicular states of linearly polarized light—has been recognized as a measure of orientation anisotropy on a molecular or submolecular scale[18–20]. Changes in orientation of different structures within a polymer, as well as morphology changes from one type of structure to another, may be driven by a macromechanical perturbation.

We have developed a versatile rheo-FTIR spectrometer that is capable both of detecting the presence of specific structures in polymer thin films and of measuring the spatial orientation of these structures simultaneously. The rheo-FTIR spectrometer collects in situ infrared absorbance and infrared linear dichroism (IRLD) spectra directly as sample films

experience a tensile deformation. One type of experiment focuses on transient orientation and relaxation responses to a well-defined, oscillatory, small-amplitude tensile deformation, as quantified in the measurement of dynamic infrared linear dichroism (DIRLD) spectra. DIRLD measurements provide information on the transient viscoelastic orientation behavior of individual moieties (e.g., crystalline or amorphous domains in semicrystalline materials, blend components, ordered mesoscale structures), thus giving a quantitative measure of each individual contribution to the overall bulk behavior. A two-dimensional correlation analysis of DIRLD spectra has also been developed to measure any interdependency between individual component responses to the applied tensile stretch[21–23]. The second type of experiment involves IRLD measurement as a sample film is subjected to large, irreversible tensile deformation. Drawing films of semicrystalline polymers to great strains may be sufficient to induce morphology changes. Any such changes will be quickly reflected in both IR absorbance and dichroism spectra as tensile strain increases. Furthermore, the effects of different morphologies on the ultimate mechanical behavior (e.g., modulus, yielding, tensile set and recovery) of sample films as they orient can be characterized. Both experiments can be performed over a range of temperatures and degrees of spectral resolution. Results for a semicrystalline isotactic polypropylene (iPP, Figure l(a)) and a thermoplastic polyurethane (TPU, Figure 1(b)), composed of "soft" prepolymer diol blocks and "hard" diisocynate blocks, are provided to illustrate the abilities of the rheo-FTIR spectrometer.

BACKGROUND

Infrared spectroscopy is used customarily for chemical identification. However, it was discovered that polarized IR light could be used to measure the amount of overall spatial orientation in cellulose fibers[20]. This technique was also used to study oriented fibrous proteins[18,19] and uniaxially drawn polyethylene fibers[24,25]. Since IR absorption involves the vibrational moments associated with chemical functionalities (e.g., C=O, C–H, C–CH_3), their spatial orientation can be measured based on the anisotropy of the absorption. Fourier transform spectroscopy succeeded the monochromator and allowed for polychromatic light sources to be used; hence, the simultaneous measurement of orientation of many functional groups was made[26,27]. To this point, only stationary (static) samples could be measured. FTIR dichroism was used to explore orientation and phase behavior of semicrystalline polymers in the solid state that had been drawn to large tensile strains[28,29]. Signal processing electronics encounter difficulty distinguishing between amplitude modulation of source radiation (due to Michelson interferometry) and

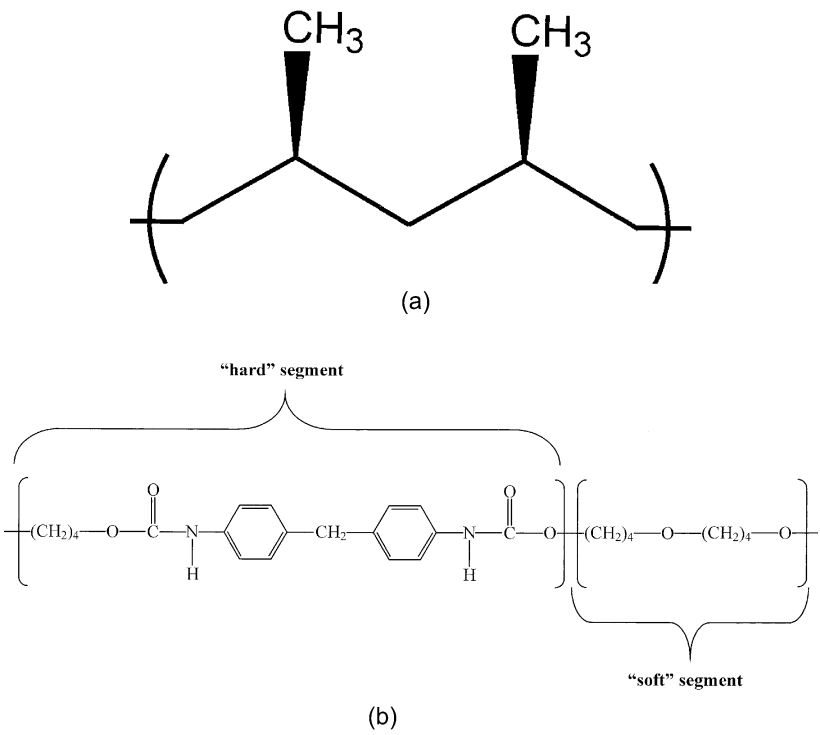

FIGURE 1 Chemical structures of polymers characterized using rheo-FTIR spectroscopy: (a) isotactic polypropylene (iPP); (b) thermoplastic polyurethane (TPU).

similar order-of-magnitude modulations (e.g., due to transience in the sample). Thus, the innovation of step-scan interferometry allowed for dynamic mechanical and optical perturbations to be imposed while retaining the benefits of a polychromatic source[30]. The ability to monitor the orientation of polymer constituents as they undergo a common perturbation (specifically, tensile stretching in the linear viscoelastic region) opened up a new area for study in polymer physics: How do individual polymer components contribute to the overall bulk behavior? The relative extent of each contribution can be quantified through IRLD.

The measurement of linear dichroism requires light that is linearly polarized in two mutually perpendicular directions. Initially, experiments involved a single linear polarizer and required two separate sets of data to be taken (then subjected to further mathematical treatment)—one with the polarizer axis at an angle of 90° relative to the other. This was

achieved by rotating either polarization optics or the sample (or both) about the axis of light propagation. The introduction of polarization modulation via a photoelastic modulator (PEM) allowed for the direct measurement of anisotropic absorbance spectra[32,33]. With this modification, dichroism may be measured directly for both stationary and transient samples.

In total, IR light from the broadband source is subjected to three successive modulations: FT (Michelson) interferometry, polarization modulation, and sample modulation. In order to extract meaningful data from a complex, triply modulated electrical signal, a rather involved demodulation scheme is required. Over the past two decades, lock-in amplifiers were used to demodulate the signal gathered by detection equipment[32,33]. One lock-in amplifier is required for each modulation imposed (a total of three for DIRLD experiments). To simultaneously extract absorbance data from the raw signal, additional lock-in amplifiers were required. More recently, digital signal processing (DSP) electronics and software algorithms have been used to replace much of the necessary demodulation hardware[34,35].

The rheo-FTIR spectrometer combines the aforementioned developments in step-scan interferometry, polarization modulation, and digital signal processing with customized rheometers to create a versatile tool for the study of structure-property relationships in polymers. The sections to follow detail the underlying principles that correlate optical property measurement with molecular orientation, followed by descriptions of the individual hardware and materials used in rheo-FTIR experiments.

THEORY

Optics and Molecular Orientation

Two criteria must be satisfied for a material to absorb light:

1. The electromagnetic frequency of incident radiation must match the oscillation frequency of the electronic dipole-transition moment of a chemical bond vibration.
2. The electric field vector of the incident radiation and the electric dipole-transition moment must be coplanar.

Many vibrational modes for polymers have energies corresponding to the mid-infrared region of the electromagnetic spectrum (wavelengths, λ, from 2.5 to 25 μm, or equivalently, wavenumbers, $\tilde{\nu}$, from 4000 to 400 cm^{-1}). If the vibrational moment associated with a given moiety is somehow oriented in a particular direction, then IR light of corresponding frequencies whose electric field vectors are polarized in the same direction will be absorbed to a greater extent than light in other

polarization states. A key relationship develops from this. Tensile stretching is expected to cause chain backbones to align with the direction of the stretch. Side chains and pendant groups may reorient as well, their precise directions fixed by geometrical relationships (due to chemical bonding) with the main chain. Vibrational moments corresponding to the main chain and side groups align accordingly. Linear dichroism is defined as the anisotropic absorption of two states of linearly polarized light[36]. Using a linear polarizer, the direction-specific absorbances, both parallel and perpendicular to a reference direction ($A_{\parallel}$ and $A_{\perp}$, respectively), may be measured.

The mathematical relationships between molecular anisotropy and optical properties have been established. Of particular use is a model developed by Hermans et al.[20], which was later used to observe specific materials by Fraser[18,19] and Stein[25], among others, that considers generalized uniaxial molecular orientation. Noda et al.[33] have shown that the orientation anisotropy may be completely described in terms of an orientation function,

$$f = \frac{3\langle \cos^2 \theta \rangle - 1}{2} \tag{1}$$

where θ is the angle between the polymer chain or group and the stretching direction[37]. The value of f varies between $-1/2$ and 1. For randomly oriented chains[38],

$$\langle \cos^2 \theta \rangle = 1/3 \quad \Rightarrow \quad f = 0 \tag{2}$$

For polymer chains oriented completely parallel to the stretch,

$$\theta = 0^\circ, \ \langle \cos^2 \theta \rangle = 1 \quad \Rightarrow \quad f = 1 \tag{3}$$

For chains oriented completely perpendicular to the stretch[39],

$$\theta = 90^\circ, \ \langle \cos^2 \theta \rangle = 0 \quad \Rightarrow \quad f = -1/2 \tag{4}$$

The orientation function may also be expressed in terms of absorption anisotropy.

$$f = \left(\frac{D-1}{D+2}\right)\left(\frac{D_\infty + 2}{D_\infty - 1}\right) = \frac{\Delta A}{\Delta A_\infty} \tag{5}$$

where D is the dichroic ratio, defined as

$$D \equiv \frac{A_{\parallel}}{A_{\perp}} \tag{6}$$

ΔA, the dichroic difference (or simply, dichroism) is defined as

$$\Delta A \equiv A_{\parallel} - A_{\perp} \tag{7}$$

and the infinity (∞) subscript denotes the case of an ideal, uniaxially oriented system. It is important to note from Equation (5) that dichroism is proportional to orientation. Thus, a quantitative relationship between a measurable quantity and the extent of physical anisotropy in a material has been established. Early IRLD studies commonly used D as a measure of optical anisotropy[18,19,25,40]. However, when either applying perturbations that cause only very small changes in the absorbance spectra or studying samples where the magnitude of D for most IR peaks nearly equals unity, ΔA provides a more sensitive measure of anisotropy. Most of the molecules exhibiting dichroic behavior give rise to ΔA values that are typically up to five orders of magnitude less than their corresponding absorbance values[33–41]. Therefore, it is very difficult to measure D with reasonably high sensitivity by simply ratioing two absorbance spectra, each with a superimposed dichroism signal of significantly less magnitude. Furthermore, an unreasonable number of scans are needed in acquiring each $A_{\parallel}$ and $A_{\perp}$ spectrum in order to measure ΔA accurately by simple subtraction (Equation (7)). This is the principal purpose of using differential spectroscopy—the direct measurement of IRLD. This is accomplished through the use of a PEM where the polarization state of the infrared beam is alternated very rapidly. The signal contribution from sample dichroism can be obtained more accurately by measuring the amplitude of a single time-dependent AC signal, rather than by subtracting two temporally different DC signals.

Rheo-Optics

A thorough synopsis of dynamic mechanical analysis and an analogous mathematical treatment of dynamic dichroism have already been given by Noda et al.[33], thus only a brief review will be given here. Tensile strain that is imposed on a thin polymer film can be represented as

$$\varepsilon = \overline{\varepsilon} + \widetilde{\varepsilon}(t) \tag{8}$$

where $\overline{\varepsilon}$ and $\widetilde{\varepsilon}$, respectively, are the static and dynamic (transient) components of the total strain, ε. For DIRLD experiments, we employ a small-amplitude oscillatory strain:

$$\widetilde{\varepsilon}(t) = \hat{\varepsilon}\sin(\varpi_s t) \tag{9}$$

From this, we expect a stress response in the form

$$\sigma = \overline{\sigma} + \hat{\sigma}\sin(\varpi_s t + \alpha) \tag{10}$$

where $\sigma, \overline{\sigma}$, and $\hat{\sigma}$ are the stress equivalents to the strain terms in Equations (8) and (9), and α is a phase angle representing some time lag between the strain stimulus and the viscoelastic stress response. The dynamic stress response may be separated into in-phase and quadrature (90° out-of-phase) components:

$$\sigma = \overline{E}\overline{\varepsilon} + E'\hat{\varepsilon}\sin(\varpi_s t) + E''\hat{\varepsilon}\cos(\varpi_s t) \tag{11}$$

where E' and E'', the dynamic tensile storage and loss moduli, respectively, are defined similarly to Young's modulus:

$$\overline{E} = \frac{\overline{\sigma}}{\overline{\varepsilon}} \tag{12}$$

$$E' = \frac{\hat{\sigma}}{\hat{\varepsilon}}\cos(\alpha) \tag{13}$$

$$E'' = \frac{\hat{\sigma}}{\hat{\varepsilon}}\sin(\alpha) \tag{14}$$

Therefore, dichroism arising from orientation anisotropy can be described as

$$\Delta A = \Delta\overline{A} + \Delta\hat{A}\sin(\varpi_s t + \beta) \tag{15}$$

$$D = \overline{D} + \hat{D}\sin(\varpi_s t + \beta) \tag{16}$$

where β represents phase lag between the strain stimulus and the dichroism response. Likewise, the dynamic component of dichroism may be separated analogously into in-phase and quadrature components:

$$\Delta A = \Delta\overline{A} + \Delta A'\sin(\varpi_s t) + \Delta A''\cos(\varpi_s t) \tag{17}$$

where $\Delta A' \equiv \Delta\hat{A}\cos(\beta)$ and $\Delta A'' \equiv \Delta\hat{A}\sin(\beta)$ are the in-phase and quadrature DIRLD spectra[42], respectively.

EXPERIMENTAL METHODS

Materials

For DIRLD experiments, thin (~30μm), biaxially drawn (~10 × machine, ~5 × transverse) isotactic polypropylene (iPP, Figure 1(a)) films are obtained directly from Manning Applied Technologies. Reflected light from the smooth film surfaces may cause artificial interference fringes and lead to erroneous signals in IR spectra. This can be remedied easily by roughing the sample surfaces with fine grit sandpaper.

The thermoplastic polyurethane (TPU, Figure 1(b)) used in static IRLD experiments consists of linear segments of 4,4-diisocyanate diphenylmethane (MDI) and tetramethylene glycol with an average molecular weight of 70,000 g/mol. The diol prepolymer blocks form the "soft segment," while the diisocyanate blocks form the so-called "hard segment" and are interconnected by the polyol. At room temperature the hard and soft segments undergo a microphase separation where the hard segments tend to aggregate into semicrystalline units. This effect is reinforced by the formation of hydrogen bonds with adjacent hard segments. TPU samples are prepared by dissolving a known amount of polymer in N,N′-dimethylformamide (DMF) at a concentration of about 20% by weight. After pouring the solution over a glass slide, the solvent is initially evaporated in a vacuum oven for 1 h at 110°C. The sample is then dried overnight at 65°C and atmospheric pressure to remove residual solvent. A hot water bath is used to aid in removing thin polymer films (approximately 20 μm thick) from the glass slide support. After a final drying cycle in a vacuum oven for another 24 h at 40°C, the sample is mounted into the rheometer without further treatment.

Instrumentation

A scheme of the complete optical and signal processing train for rheo-FTIR experiments is given as Figure 2. Below, details are given about important components involved in the optical train. The spectrometer, PEM, rheometers, detector, and other optics are placed on a vibration-isolated optical table (Newport Corporation). Details regarding the signal processing train, the collection and application of appropriate background and calibration spectra, and other hardware parameters are given in the Appendix.

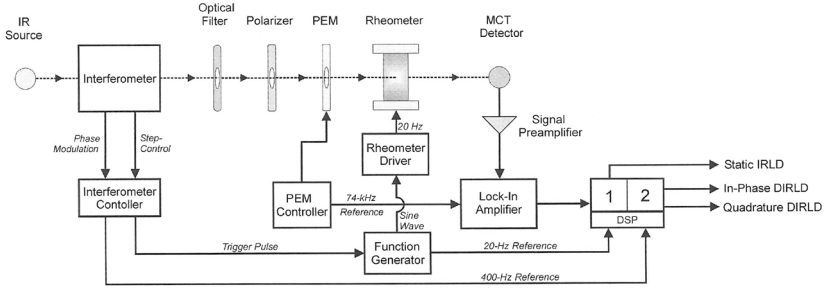

FIGURE 2 Schematic diagram of rheo-FTIR optical and signal processing trains.

FTIR Spectrometer

For all experiments, an FTIR spectrometer (Bio-Rad FTS 6000) is used and essentially serves as a polychromatic infrared source. The instrument is equipped with a Michelson interferometer capable of operating in both continuous ("rapid") and step-scan modes. The interferometer is coupled with a fast, liquid nitrogen cooled mercury-cadmium-telluride (MCT) detector. A step-scanning interferometer is necessary because, in conventional continuous-scan mode, the interferogram itself is time-dependent; hence, its signal modulation may overlap with other time-dependent phenomena. This would present difficulty in separating other transient responses from the interferometric modulation of the IR beam. The instrument is also capable of performing time-resolved data collection—useful for stress relaxation experiments.

For DIRLD experiments, a low-frequency phase modulation is imposed on the source by "dithering" (oscillating) the interferometer moving mirror about each retardation step. This helps to improve signal-to-noise ratio for the relatively diminutive DIRLD response in three ways:

1. It moves the dichroism signal into a frequency response range that is appropriate for the MCT detector.
2. It reduces the dynamic range of the signal.
3. It modulates all IR wavenumbers at a common electrical frequency.

The stepping frequency, phase modulation frequency, and phase modulation amplitude of the moving mirror are adjustable parameters.

Upon traversing the interferometer, the recombined, modulated beam is directed out of the spectrometer through an external port using plane mirrors. This slightly divergent beam is redirected using a gold-coated parabolic mirror (6.5-inch focal length), which sends the light, sequentially, through an optical low-pass filter[43], a rotatable wire grid polarizer[44], the PEM, and onto the sample (positioned at the mirror focal point), where it is finally transmitted through to the detector.

Photoelastic Modulator (PEM)

A photoelastic modulator (PEM-90/ZS37, Hinds Instruments, Inc.) is used to generate broadband polarization modulation in the mid-infrared electromagnetic region. This modulation also serves as a high-frequency carrier wave for the sample dichroism signal and increases the signal-to-noise ratio because of multiplicative noise suppression due to averaging. The operation of the PEM is based on a mechanically stressed zinc selenide (ZnSe) crystal, which exhibits oscillating retardation according to the amplitude of an applied voltage. The fundamental oscillation frequency of the PEM is fixed at a value of $\varpi_{PEM} \approx 37\,\text{kHz}$. For all experiments, the PEM is set to one-half wave retardation with a center

wavenumber of 1500 cm^{-1}. As a result, the IR beam alternates between orthogonal plane polarized states at a frequency of $2\varpi_{PEM}$, therefore, the desired dichroism signal can be detected at a frequency of approximately 74 kHz.

Mechanical

Tensile rheometers are used to apply a mechanical perturbation to sample films, thus inducing molecular reorientation. Depending on the magnitude and type of strain we wish to impose, one of two rheometers is used.

Dynamic rheometer. For DIRLD experiments, a custom-built micro-rheometer (TC-100 Polymer Modulator, Manning Applied Technology) is used to apply a precise, reproducible, small-amplitude oscillatory strain. Sample films are mounted using two jaws—one stationary, one attached to piezo drivers that supply the strain. Sensors attached to the piezoelectric heads allow for measurement of displacement of the moving jaw (strain) and also the tensile force applied to the sample (stress). The total static elongation capacity of the dynamic rheometer is 25 mm, and the dynamic elongation amplitude ($\alpha\ \hat{\varepsilon}$) can be adjusted up to 75 μm. To ensure an elastic, reversible, optically linear response from sample films, dynamic elongation amplitude is kept below 0.5% of the film gauge length. Since the drive mechanism is piezoelectric, the dynamic rheometer is capable of producing any arbitrary waveform with a variable frequency from 0.5 to 50 Hz[45]. A programmable function generator (Hewlett Packard 33120 A) controls the waveform and the modulation frequency. For DIRLD experiments, a 20-Hz sinusoidal waveform is used. To ensure precise data acquisition, the interferometer controller synchronizes the interferometer, the function generator, and, subsequently, the dynamic rheometer. Using forced air convection, the dynamic rheometer can provide nearly isothermal conditions for temperatures ranging from ambient to 70°C. Potassium bromide (KBr) windows are used both to thermally insulate the sample chamber and to provide a transparent medium for the IR beam. However, it is difficult to obtain meaningful data for wavenumbers less than 650 cm^{-1}, because the MCT detector cuts off near this point.

Static rheometer. For static IRLD experiments, a strain rheometer (Minimat 2000, Rheometric Scientific, Inc.) is used to tensile draw sample films irreversibly to large strains. Samples are stretched in stepwise increments at an elongation rate of 0.5 mm/min. At each strain step, drawing is paused while spectra are collected. The static rheometer is capable of drawing in increments of 0.3 μm up to 100 mm total displacement at elongation rates up to 100 mm/min. Furthermore, a custom-modified environmental chamber is used to provide good

temperature control ranging from ambient conditions to 200°C, although this modification limits total displacement to 45 mm. This rheometer has also been modified with KBr windows to allow measurement of IR spectra. To minimize signal loss due to beam divergence, the rheometers are placed with their sample contents at the focal point of the parabolic mirror and as close as possible to the optics immediately surrounding them.

RESULTS AND DISCUSSION

Small-Amplitude Dynamic Deformation (DIRLD of iPP)

To review, inferences may be drawn from DIRLD spectra regarding which constituent moieties dominate the overall linear viscoelastic response of iPP. Static IRLD spectra may be used to track any changes in morphology and orientation as a sample film undergoes large, irreversible deformation. Figure 3 shows an IR absorbance spectrum for iPP. While 19 peaks can be observed distinctly, the present discussion will focus only on those peaks showing clear, strong dichroism responses. Table I lists characteristic IR peaks of interest and the vibrational

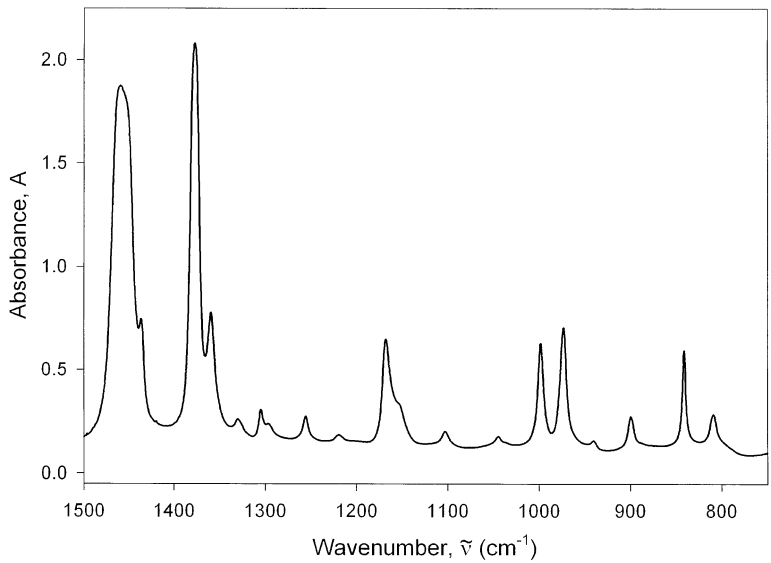

FIGURE 3 Infrared absorbance spectrum of isotactic polypropylene (25°C, 1 cm^{-1} resolution, 1024 scans co-added).

mode(s) to which they are commonly attributed[46–51]. It should be noted that a single IR peak might be composed of multiple vibrational dipole moments.

$\Delta A'(\tilde{\nu})$ and $\Delta A''(\tilde{\nu})$ spectra of iPP at three different temperatures are shown in Figure 4. Every dichroism signal (on the order of 10^{-4} absorbance units) can be distinguished clearly from background noise. For all temperatures, $\Delta A'(\tilde{\nu})$ is, at most wavenumbers, at least an order of magnitude greater than $\Delta A''(\tilde{\nu})$. A greater orientation response from the in-phase elastic component of dichroism is expected (Figure 4(a)) because the sample is in a solid (i.e., rubbery) state. The qualitative nature of the

TABLE I Characteristic infrared absorbance peaks of isotactic polypropylene.

Wavenumber (cm^{-1})[a]	Vibrational mode(s)	Associated micro-structure	Dipole moment orientation
809	C–C stretching Coupled C–H deformation	Helical (α-crystalline)	Perpendicular (⊥)
841 (S)	C–C stretching CH_2 rocking CH_3 rocking	Helical (α-crystalline and mesomorphic)	Parallel (∥)
900	C–C stretching Coupled C–H deformation	Helical (α-crystalline)	Perpendicular (⊥)
941 (w)	C–C stretching Coupled C–H deformation		Perpendicular (⊥)
973	C–C stretching CH_2 rocking CH_3 rocking	Amorphous	Parallel (∥)
998 (S)	C–C stretching CH_2 rocking CH_3 rocking	Helical (α-crystalline)	Parallel (∥)
1153 (sh)	CH_3 wagging	Amorphous	Parallel (∥)
1167 (S)	C–C stretching CH_3 wagging	Crystalline	Parallel (∥)
1257 (w)	C–H wagging		Parallel (∥)
1305	C–H bending		Parallel (∥)
1359	C–H bending	Crystalline	Perpendicular (⊥)
1377 (S)	Symmetric C–H bending	Amorphous	Perpendicular (⊥)
1436	CH_2 bending		Perpendicular (⊥)
1459 (S)	Asymmetric, in-plane CH_3 bending	Amorphous	Perpendicular (⊥)

[a]Relative intensity: S = strong, w = weak, sh = shoulder.

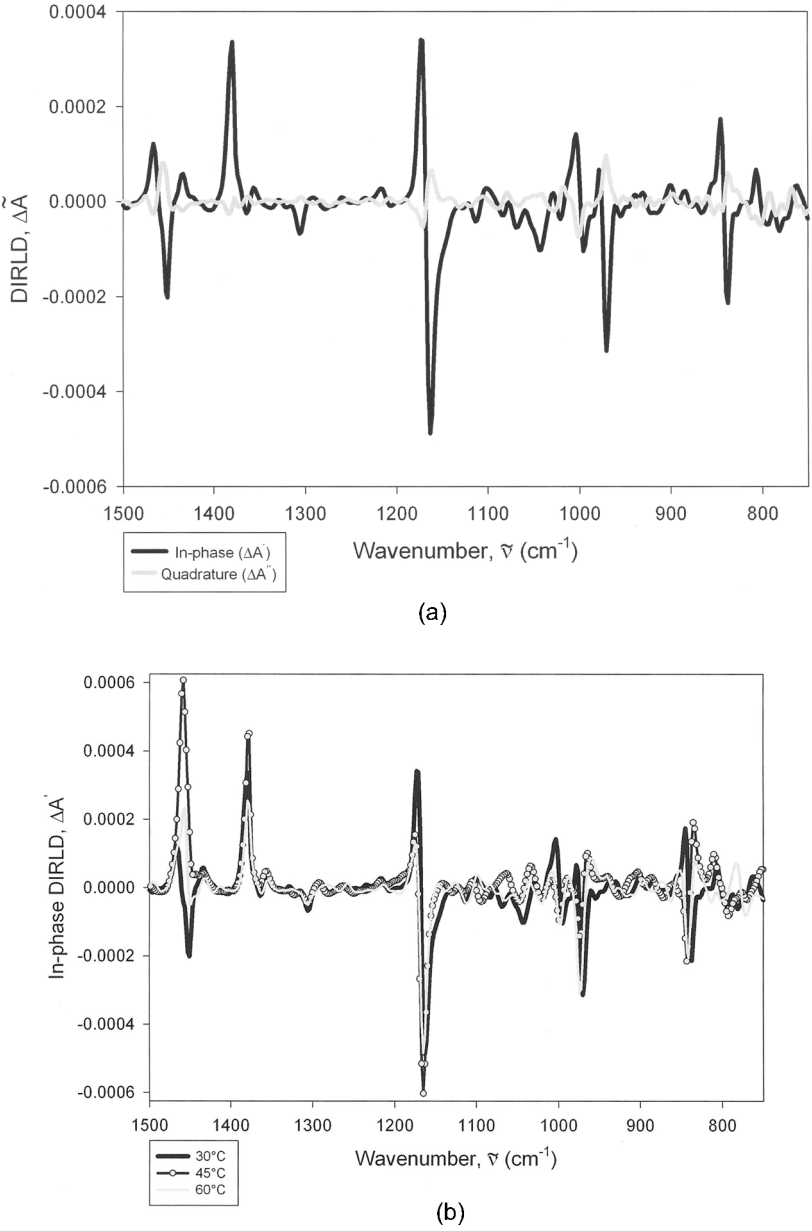

FIGURE 4 DIRLD spectra of iPP under reversible oscillatory tensile strain: (a) in-phase vs. quadrature at 30°C; (b) in-phase at 30, 45, and 60°C; (c) quadrature at 30, 45, and 60°C.

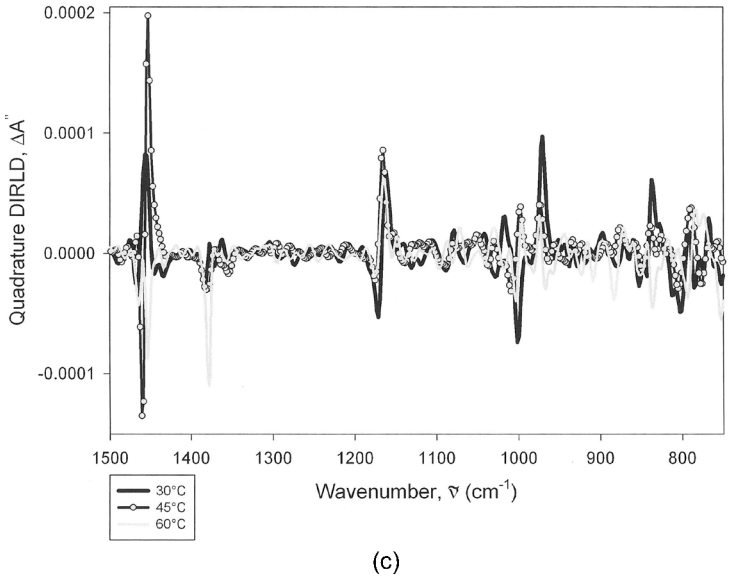

FIGURE 4 Continued.

DIRLD spectra does not vary much over different temperatures, yet their magnitudes are different. As might be expected, the extent of orientation (i.e., magnitude of $\Delta\widetilde{A}(\widetilde{\nu})$) decreases for greater temperatures (Figures 4(b) and 4(c)), most likely due to a faster overall relaxation in the sample during deformation, especially for chains in the amorphous regions.

The sign of a dichroism peak is based on the orientations of its associated vibrational moments with respect to the stretching direction. Moments oriented perfectly parallel with the direction of applied strain will give a maximum positive dichroism response. Likewise, moments oriented at 90° with respect to the stretch give rise to a maximum negative dichroism signal. In response to a small deformation, DIRLD peaks can exhibit either a purely isotropic (Lorentzian) shape (e.g., $\Delta A'(1167\,\mathrm{cm}^{-1})$ in Figure 4(a)) or a bimodal shape (e.g., $\Delta A'(1377\,\mathrm{cm}^{-1})$ in Figure 4(a)). Bimodal DIRLD peaks manifest due to a small shift in the horizontal (wavenumber) position of certain absorbance peaks as strain is applied[41]. This bimodal splitting illustrates the fact that certain peaks are influenced by multiple vibrational dipoles. The magnitudes of $\Delta A'$ for crystalline ($\widetilde{\nu} = 841,\ 997,\ 1167\,\mathrm{cm}^{-1}$) and amorphous ($\widetilde{\nu} = 973,\ 1377,\ 1457\,\mathrm{cm}^{-1}$) domains are quite comparable. We suggest that this is due to an offsetting balance between the relative amount present and orientation response strength of each domain. The iPP sample used for dynamic experiments is known to possess a maximum crystallinity of 15%. Thus,

we suggest that the quantitative similarity of crystalline and amorphous $\Delta A'$ peaks arises from the presence of a large amount of amorphous chains that show only a slight amount of orientation and, at the same time, a less plentiful population of crystalline domains that shows a much greater instantaneous orientation response. This physical description is intuitive because crystalline domains will orient first and to a greater degree than noncrystalline domains in the elastic deformation region. In the mechanical yielding and plastic deformation regions, the dichroism responses of crystalline and amorphous domains are expected to be quite different. Indeed, this is observed for iPP films that are tensile deformed to large strains[52]. At about 50% strain, iPP yields. This event is accompanied by a saturation (maximization) of the crystalline dichroism response and a simultaneous jump in amorphous domain dichroism. Beyond the yield point, amorphous domains continue to orient and dominate the iPP dichroic response, while the crystalline response remains saturated.

Large Static Deformation (IRLD of TPU)

The capabilities of the rheo-FTIR spectrometer while operating in large, irreversible deformation mode are illustrated using a thermoplastic polyurethane (TPU) film. The FTIR spectrum of TPU (Figure 5) is rich with absorption peaks arising from the chemical moieties and their

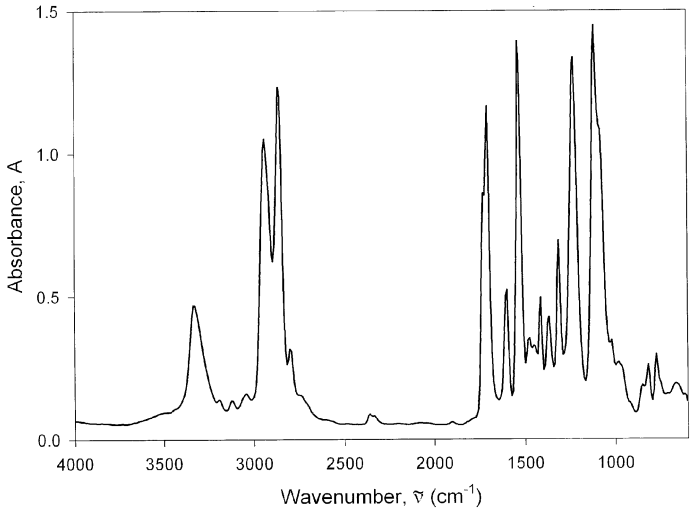

FIGURE 5 IR absorbance spectrum of TPU (25°C, 8 cm^{-1} resolution).

TABLE II Characteristic infrared absorbance peaks of thermoplastic polyurethane.

Wavenumber (cm^{-1})[a]	Vibrational mode(s)[b]	Associated micro-structure(s)	Dipole moment orientation
1072 (S)	ν(C–O–C) urethane + ester	Interface	Parallel ($\parallel$)
1111 (S)	ν(C–O–C) ester	Soft	Parallel ($\parallel$)
1228 (S)	ν(C–N) + δ(N–H)	Hard	Perpendicular ($\perp$)
1311 (m)	ν(C–N) + δ(N–H), phenyl	Hard	Perpendicular ($\perp$)
1367 (w)	$\omega(CH_2)$ glycol	Soft	Parallel ($\parallel$)
1413 (w)	ν(C–C) phenyl ring	Hard	
1472 (w)	$\delta(CH_2)$	Soft	Parallel ($\parallel$)
1532 (S)	ν(C–N) + δ(N–H)	Hard	Perpendicular ($\perp$)
1600 (m)	ν(C=C)	Hard	
1706 (S)	ν(C=O)	Interface	Perpendicular ($\perp$)
1733 (S)	ν(C=O)	Interface	Perpendicular ($\perp$)
2859 (S)	ν(C=H)	Interface	
2939 (S)	ν(C–H)	Interface	
3329 (S)	ν(N–H)	Hard	Perpendicular ($\perp$)

[a]Relative intensity: S = strong, m = medium, w = weak.
[b]ν = stretching mode, ω = wagging mode, δ = bending mode.

interactions (Table II)[53]. The vibrational modes can be assigned to either the soft segment, hard segment, or the interface. The sample film is stretched uniaxially using the static rheometer, and the spectra are recorded as a function of tensile deformation. In fact, we are able to monitor the quantitative dichroic response of all the vibrational modes listed in Table II simultaneously, as shown in Figure 6.

The dichroic response from all the vibrational moments in each domain falls into one of two categories: those showing either a strong response (quantitatively similar to the C–O–C or C–N response) or a weak response (similar to C–H or N–H). Therefore, only three curves are reported for each domain. In the soft domain (Figure 7(a)), it appears that there are two types of responses. The responses of the C–H stretching vibration ($\tilde{\nu} = 2859,\ 2939\,cm^{-1}$) increase in magnitude with tensile strain, ultimately reaching a value of $\Delta\overline{A} \approx -1.5 \times 10^{-3}$. On the other hand, the response at the C–O–C stretching vibration ($\tilde{\nu} = 1111\,cm^{-1}$) is much stronger and reaches a value of $\Delta\overline{A} \approx 5 \times 10^{-3}$ at 550% strain. Since the C–O–C stretching vibration will be oriented along the backbone, it has a large dichroism response when the backbone orients strongly in response to the applied strain. The weaker response of the C–H stretch (in the soft domain) indicates that even though the chain

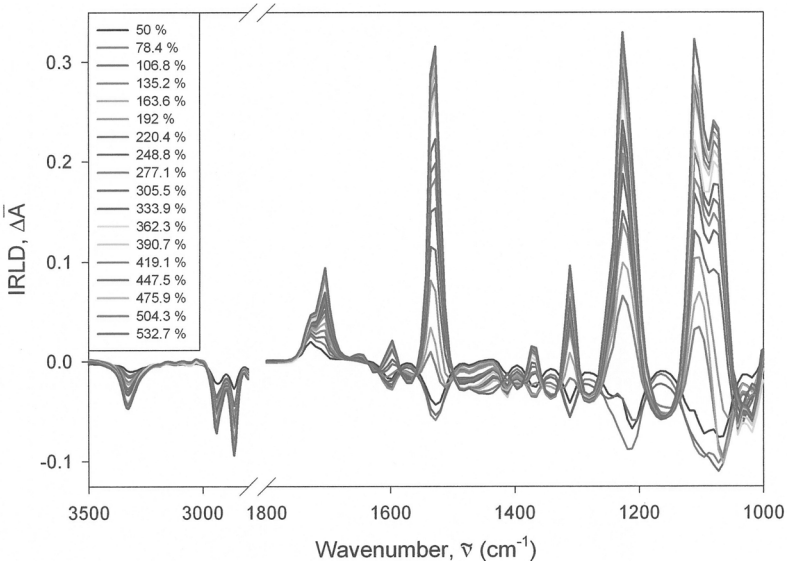

FIGURE 6 IRLD spectra of TPU under static, irreversible tensile strain (25°C, 8 cm^{-1} resolution).

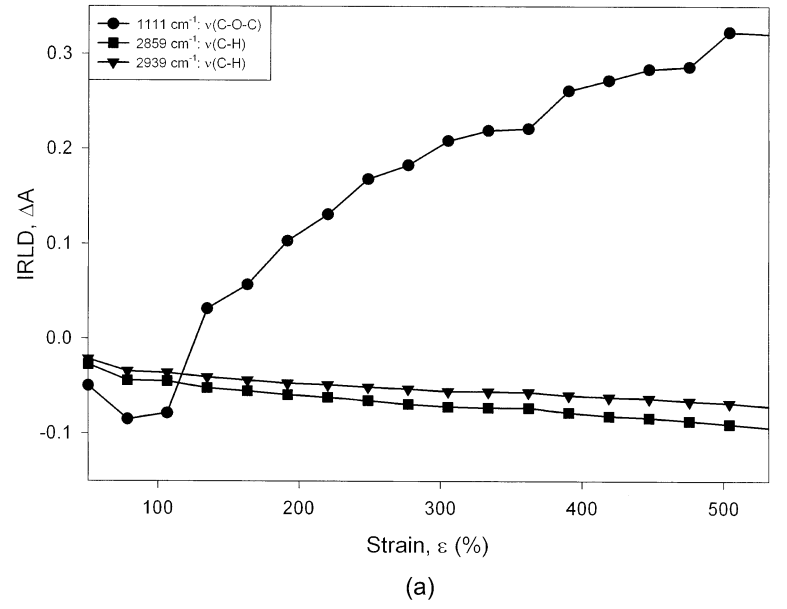

FIGURE 7 Quantitative IRLD response of selected vibrational modes associated with TPU microdomains: (a) soft domains; (b) hard domains.

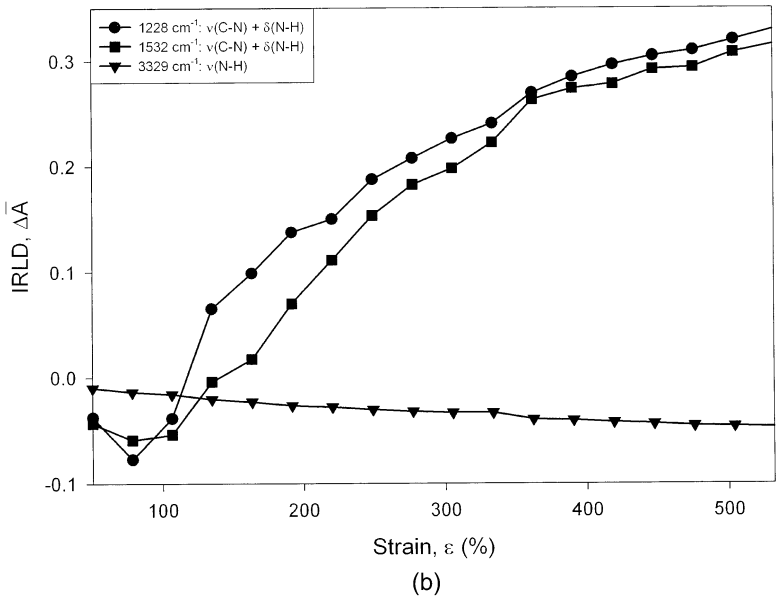

FIGURE 7 Continued.

as a whole is orienting, the dichroism response from the C–H side chains is not strong. This could be because:

1. This dipole moment is perpendicular to the orientation direction. The C–H stretch would be less sensitive to overall orientation of the backbone, since, even after significant backbone orientation, the dipole moment could still be more or less randomly oriented. For strong orientation correlation between backbone and side group vibrational moments, a near perfect orientation of the main chain is required.
2. The C–H side chains have a faster relaxation time than the main chain. Thus, some degree of relaxation may even occur during IRLD measurement.

The response of the hard domain is somewhat similar (Figure 7(b)) The N–H stretching vibration ($\tilde{\nu} = 3329\,\text{cm}^{-1}$) shows a weaker response compared to that of the ν(C–N) + δ(N–H) modes ($\tilde{\nu} = 1228, 1532\,\text{cm}^{-1}$). The C–N stretch appears to be more sensitive to hard domain orientation. As can be seen from Figure 1(b), this vibration is located along the backbone chain in the hard domain (i.e., its dipole moment is parallel to the orientation direction). Thus, ν(C–N) is more sensitive to hard domain orientation than the δ(N–H) moment, which is perpendicular to the stretch.

CONCLUSION AND FUTURE WORK

These measurements illustrate the power of the Rheo-FTIR spectrometer in simultaneously measuring direct, quantitative, simultaneous responses of multiple vibrational dipoles over a wide range of temperatures and deformation modes. By combining elements of spectroscopy, polarimetry, rheometry, and digital signal processing, it is possible to measure, both directly and sensitively, the overall orientation behavior of components within complex polymers. The application of this instrument toward characterizing the morphology and viscoelastic orientation behavior of other polymer materials is ongoing. The following is a brief introduction to semicrystalline, stereospecific polypropylenes that possess unique and interesting microstructures and physical properties, which are highly responsive to the effects of mechanical and thermal processing. The recent use of metallocene catalysts[54–56] to generate highly stereospecific vinyl polymers has sparked renewed interest in their fundamental research. Our current efforts focus on elastomeric semi-syndiotactic and isotactic polypropylenes.

Syndiotactic polypropylene (sPP) exhibits a rich polymorphism that can be manipulated through thermal processing and mechanical deformation. To date, five distinct polymorphs, including four crystalline forms[57–65] and a semi-ordered, paracrystalline, mesomorphic form ("mesophase"[66]), have been identified. This mesophase is thought to be responsible for elastomeric behavior in sPP as it is tensile drawn to large strains ($\varepsilon > 400\%$)[67–71]. While characterization of highly syndiotactic sPP is ongoing, very little is known about the relationship between stereoregularity and physical properties. We are studying metallocene-catalyzed materials that possess different degrees of syndioregularity (i.e., semi-syndiotactic polypropylenes, or semi-sPP). This presents a unique opportunity to characterize sPP using rheo-optical FTIR spectroscopy, as well as other complementary techniques, with tacticity as a variable. Our preliminary work suggests that for melt-quenched films, the kinetics of deformation-induced formation and orientation of the mesophase[72] and aging behavior (i.e., crystallization kinetics)[73] are remarkably slower as syndiotacticity decreases.

Metallocene catalysts have also been used to synthesize a highly elastomeric, "stereoblock," isotactic-atactic polypropylene (ePP)[74–76] that can be solvent-extracted into fractions of varying tacticity and crystallinity. In situ birefringence and X-ray scattering data for ePP show a crystalline-to-mesomorphic microstructural transformation as the film is tensile drawn, similar to sPP[77–80]. In addition to confirming the presence and orientation behavior of iPP crystal morphs and mesomorphs (as observed with rheo-birefringence, small-angle, and wide-angle X-ray scattering), the rheo-FTIR spectrometer will provide equivalent information for the amorphous atactic segments simultaneously.

The instrument is also being used to characterize thermoplastic polyurethane with dispersed styrene acrylonitrile (SAN) nanospheres and component dynamics in copolymers and miscible compatible blends (e.g., PS/PVME, high-MW *d*-PS/low-MW PS).

REFERENCES AND NOTES

[1] Ferrer-Balas, D., M. Ll. Maspoch, A. B. Martinez, and O. O. Santana. (2001). Influence of annealing on the microstructural, tensile and fracture properties of polypropylene films. *Polymer* **42**, 1697–1705.

[2] Uzomah, T. C. and S. C. O. Ugbolue. (1997). Time and temperature effects on the tensile yield properties of polypropylene. *J Appl. Polym. Sci.* **65**, 625–633.

[3] Bryant, J. E. and W. R. Burghardt. (2002). Extension of axisymmetric flow birefringence to a time-dependent stagnation flow. *J Non-Newton. Fluid Mech.* **108**, 257–273.

[4] Chand, S., G. S. Bhat, J. E. Spruiell, and S. Malkan. (2001). Structure and properties of polypropylene fibers during thermal bonding. *Thermochim. Acta* **357–368**, 155–160.

[5] Archer, L. A. and G. G. Fuller. (1994). Pattern and segment relaxation in a block copolymer melt following step shear flow. *Macromolecule* **27**, 7152–7156.

[6] Lodge, T. P. (1994). In *Rheology: Principles, Measurements, and Applications*, ed. C. W. Macosko. New York: Wiley-VCH, pp. 379–421.

[7] Caputo, F. E., W. R. Burghardt, K. Krishnan, F. S. Bates, and T. P. Lodge. (2002). Time-resolved small-angle X-ray scattering measurements of a polymer bicontinuous microemulsion structure factor under shear. *Phys. Rev. E* **66**, 041–401.

[8] Caputo, F. E., V. M. Ugaz, W. R. Burghardt, and J. F. Berret. (2002). Transient 1-2 plane small-angle X-ray scattering measurements of micellar orientation in aligning and tumbling nematic surfactant solutions. *J. Rheol.* **46**, 927–946.

[9] Vaish, N., D. K. Cinader, W. R. Burghardt, W. Zhou, and J. A. Korufield. (2001). Molecular orientation in quenched channel flow of a flow aligning main chain thermotropic liquid crystalline polymer. *Polymer* **42**, 10147–10153.

[10] Burghardt, W. R., F. E. Caputo, K. Krishnan, F. S. Bates, and T. P. Lodge. (2001). Small-angle neutron, X-ray, and light scattering studies of a polymer bicontinuous microemulsion under shear. *Abstr. Pap. Am. Chem. Soc.* **222**, 165-PMSE.

[11] Caputo, F. E. and W. R. Burghardt. (2001). Real-time 1-2 plane SAXS measurements of molecular orientation in sheared liquid crystalline polymers *Macromolecules* **34**, 6684–6694.

[12] Thomann, R., J. Kressler, S. Setz, C. Wang, and R. Mülhaupt. (1996). Morphology and phase behaviour of blends of syndiotactic and isotactic polypropylene: 1. X-ray scattering, light microscopy, atomic force microscopy, and scanning electron microscopy. *Polymer* **37**, 2627–2634.

[13] Huang, K., L. A. Archer, and G. G. Fuller. (1996a). Polarization-modulated Raman scattering measurements of nematic liquid crystal orientation. *Rev. Sci. Instrum.* **67**, 3924–3930.

[14] Huang, K., L. A. Archer, and G. G. Fuller. (1996b). Microstructural dynamics of a homopolymer melt investigated using two-dimensional Raman scattering. *Macromolecules* **29**, 966–972.

[15] Archer, L. A. and G. G. Fuller. (1994). Segment orientation in a quiescent block copolymer melt studied by Raman scattering. *Macromolecules* **27**, 4359–4363.

[16] Archer, L. A., K. Huang, and G. G. Fuller. (1994). Orientation dynamics of a polymer melt studied by polarization-modulated laser Raman-scattering. *J. Rheol.* **38**, 1101–1125.
[17] Archer, L. A., G. G. Fuller, and L. Nunnelley. (1992). Dynamics of polymeric liquids using polarization-modulated laser Raman-scattering. *Polymer* **33**, 3574–3581; **34**, 1344.
[18] Fraser, R. D. B. (1956). Interpretation of infrared dichroism in fibrous proteins—the 2μ region. *J. Chem. Phys.* **24**, 89–95.
[19] Fraser, R. D. B. (1953). The interpretation of infrared dichroism in fibrous protein structures. *J. Chem. Phys.* **21**, 1511–1515.
[20] Hermans, J. J., P. H. Hermans, D. Vermaas, and A. Weidinger. (1946). Quantitative evaluation of orientation in cellulose fibres from the X-ray fibre diagram. *Rec. Trav. Chim. Pays-Bas* **65**, 427–447.
[21] Noda, I. (1990). Two-dimensional infrared (2D IR) spectroscopy: Theory and applications. *Appl. Spectrosc.* **41**, 550–561.
[22] Noda, I., A. E. Dowrey, and C. Marcott. (1993). Recent developments in two-dimensional infrared (2D IR) correlation spectroscopy. *Appl. Spectrosc.* **47**, 1317–1323.
[23] Pézolet, M., C. Pellerin, R. E. Prud'homme, and T. Buffeteau. (1998). Study of polymer orientation and relaxation by polarization modulation and 2D-FTIR spectroscopy. *Vib. Spectrosc.* **18**, 103–110.
[24] Stein, R. S. and F. H. Norris. (1956). The X-ray diffraction, birefringence, and infrared dichroism of stretched polyethylene. *J. Polym. Sci.* **21**, 381–396.
[25] Stein, R. S. (1958). The X-ray diffraction, birefringence, and infrared dichroism of stretched polyethylene. II: Generalized uniaxial crystal orientation. *J. Polym. Sci.* **31**, 327–334.
[26] Siesler, H. W. (1993). In *Structure-Property Relations in Polymers: Spectroscopy and Performance*, eds. M. W. Urban and C. D. Craver. Washington, D.C.: American Chemical Society, pp. 64–77.
[27] Siesler, H. W. (1985). Rheo-optical Fourier-transform infrared-spectroscopy of polymers. 9: Stretching-induced II(α)-I(β) crystal phase-transformation in poly(vinylidene fluoride). *J. Polym. Sci. Part B Polym. Phys.* **23**, 2413–2422.
[28] Hendra, P. J. and W. F. Maddams. (1996). In *Polymer Spectroscopy*, ed. A. H. Fawcett. New York: John Wiley, pp. 173–202.
[29] Young, R. J. (1996). In *Polymer Spectroscopy*, ed. A. H. Fawcett. New York: John Wiley, pp. 203–229.
[30] Crocombe, R. A. and S. V. Compton. The design, performance and applications of a dynamically-aligned step-scan interferometer. Unpublished work. Hercules, Calif.: Bio-Rad Laboratories.
[31] Green, M. J., B. J. Barner, and R. M. Corn. (1991). Real-time sampling electronics for double modulation experiments with Fourier transform infrared spectrometers. *Rev. Sci. Instrum.* **62**, 1426–1430.
[32] Marcott, C. (1984). Linear dichroism of polymer-films using a polarization-modulation Fourier-transform infrared technique. *Appl. Spectrosc.* **38**, 442–443.
[33] Noda, I., A. E. Dowrey, and C. Marcott. (1988). A spectrometer for measuring time-resolved infrared linear dichroism induced by a small-amplitude oscillatory strain. *Appl. Spectrosc.* **42**, 203–216.
[34] Curbelo, R. Digital signal processing (DSP) applications in FT-IR: Implementation examples for rapid and step scan systems. Unpublished work. Hercules, Calif.: Bio-Rad Laboratories.

[35] Drapcho, D. L., R. Curbelo, E. Y. Jiang, R. A. Crocombe, and W. J. McCarthy. (1997). Digital signal processing for step-scan Fourier transform infrared photoacoustic spectroscopy. *Appl. Spectrosc.* **51**, 453–460.
[36] Hecht, E. (1988). *Optics*, 3rd ed., Reading, Mass.: Addison Wesley Longman, p. 327.
[37] This assumes that vibrational dipoles are parallel to their associated chains.
[38] For a randomly oriented (i.e., isotropic) material, there is an equal chance for a chain to lie along any one of three dimensional axes.
[39] Chains aligned perpendicular to the reference have an equal chance of being aligned with one of two unique orthogonal axes: in the plane of polarization or along the axis of propagation.
[40] Schmidt, P. G. (1963). Polypropylene structure. *J. Polym. Sci. Part A* **1**, 2317–2325.
[41] Frisk, S., R. M. Ikeda, J. F. Rabolt, and D. B. Chase. (2000). Band shifts in the dynamic infrared spectra of oriented isotactic polypropylene. *Abstr. Pap. Am. Chem. Soc.* **220**, 200–PMSE.
[42] To be sure, both $\Delta A'$ and $\Delta A''$ are functions of wavenumber, that is, $\Delta\mathrm{A}\ \Delta A' = \Delta A'(\tilde{\nu})$ and $\Delta A'' = \Delta A''(\tilde{\nu})$.
[43] This anti-aliasing filter discards wavenumbers greater than $2000\,\mathrm{cm}^{-1}$, thus allowing the use of undersampling to reduce data acquisition time.
[44] A convention is chosen where the polarization axis is aligned parallel with respect to the stretching direction.
[45] This limitation arises due to the Win-IR Pro software, not the dynamic rheometer itself.
[46] Wang, H., R. A. Palmer, and C. J. Manning. (1997). Study of impulse polymer rheooptics by step-scan FT-IR time-resolved spectroscopy. *Appl. Spectrosc.* **51**, 1245–1250.
[47] Luongo, J. P. (1960). Infrared study of polypropylene. *J. Appl. Polym. Sci.* **3**, 302–309.
[48] McDonald, M. P. and I. M. Ward. (1961). The assignment of the infra-red absorption bands and the measurement of tacticity in polypropylene. *Polymer* **2**, 341–355.
[49] Snyder, R. G. and J. H. Schachtschneider. (1964). Valence force calculation of the vibrational spectra of crystalline isotactic polypropylene and some deuterated polypropylenes. *Spectrochim. Acta* **20**, 853–863.
[50] Koenig, J. C. (1980). *Chemical Microstructure of Polymer Chains*. New York: Wiley, p. 341.
[51] Kissen, Y. V. (1974). Structures of copolymers of high olefins. *Adv. Polym. Sci.* **15**, 92–155.
[52] Parthasarthy, G., M. S. Sevegney, and R. M. Kannan. (2002). Rheooptical Fourier transform infrared spectroscopy of the deformation behavior in quenched and slow-cooled isotactic polypropylene films. *J. Polym. Sci. Part B Polym. Phys.* **40**, 2539–2551.
[53] Wang, H., D. K. Graff, J. R. Schoonover, and R. A. Palmer. (1999). Static and dynamic infrared linear dichroism study of a polyester/polyurethane copolymer using step-scan FTIR and a photoelastic modulator. *Appl. Spectrosc.* **53**, 687–696.
[54] Ewen, J. A., R. L. Jones, and A. Razavi. (1988). Syndiospecific propylene polymerizations with group 4 metallocenes. *J. Am. Chem. Soc.* **110**, 6255–6256.
[55] Longo, P., A. Proto, A. Grassi, and P. Ammendola. (1991). Stereospecific polymerization of propylene in the presence of homogeneous catalysts: Ligand-monomer enantioselective interactions. *Macromolecules* **24**, 4624–4625.
[56] Grisi, F., P. Longo, A. Zambelli, and J. A. Ewen. (1999). Group 4 C_s symmetric catalysts and 1-olefin polymerization. *J. Mol. Catal. A Chem.* **140**, 225–233.

[57] Lotz, B., A. J. Lovinger, and R. E. Cais. (1988). Crystal structure and morphology of syndiotactic polypropylene single crystals. *Macromolecules* **21**, 2375–2382.
[58] Lovinger, A. J., B. Lotz, and D. D. Davis. (1990). Interchain packing and unit cell of syndiotactic polypropylene. *Polymer* **31**, 2253–2259.
[59] Auriemma, F., C. De Rosa, O. Ruiz de Ballesteros, and P. Corradini. (1997). Kink bands in form II of syndiotactic polypropylene. *Macromolecules* **30**, 6586–659l.
[60] De Rosa, C., F. Auriemma, and V. Vinti. (1998). On the form II of syndiotactic polypropylene. *Macromolecules* **31**, 7430–7435.
[61] Auriemma, F., R. Born, H. W. Spiess, C. De Rosa, and P. Corradini. (1995). Solid-state ^{13}C-NMR investigation of the disorder in crystalline syndiotactic polypropylene. *Macromolecules* **28**, 6902–6910.
[62] Natta, G., P. Corradini, and P. Ganis. (1960). Chain conformation of polypropylenes having a regular structure. *Makromol. Chem.* **39**, 238–242.
[63] Natta, G., M. Peraldo, and G. Allegra. (1964). Crystalline modification of syndiotactic polypropylene having a zig-zag chain conformation. *Makromol. Chem.* **75**, 215–216.
[64] Chatani, Y., H. Maruyama, T. Asanuma, and T. Shiomura. (1991). Structure of a new crystalline phase of syndiotactic polypropylene. *J. Polym. Sci. Polym. Phys. Ed.* **29**, 1649–1652.
[65] Auriemma, F., C. De Rosa, O. Ruiz de Ballesteros, V. Vinti, and P. Corradini. (1998). On the form IV of syndiotactic polypropylene. *J. Polym. Sci. Part B Polym. Phys.* **36**, 395–402.
[66] Vittoria, V., L. Guadagno, A. Comotti, R. Simonutti, F. Auriemma, and C. De Rosa. (2000). Mesomorphic form of syndiotactic polypropylene. *Macromolecules* **33**, 6200–6204.
[67] Auriemma, F., O. Ruiz de Ballesteros, and C. De Rosa. (2001). Origin of the elastic behavior of syndiotactic polypropylene. *Macromolecules* **34**, 4485–4491.
[68] De Rosa, C., M. C. Gargiulo, F. Auriemma, O. Ruiz de Ballesteros, and A. Razavi. (2002). Elastic properties and polymorphic behavior of fibers of syndiotactic polypropylene at different temperatures. *Macromolecules* **35**, 9083–9095.
[69] Guadagno, L., C. D'Aniello, C. Naddeo, and V. Vittoria. (2000). Polymorphism of oriented syndiotactic polypropylene. *Macromolecules* **33**, 6023–6030.
[70] Guadagno, L., C. D'Aniello, C. Naddeo, and V. Vittoria. (2001). Structure and physical properties of syndiotactic polypropylene oriented from different polymorphs. *Macromolecules* **34**, 2512–2521.
[71] Guadagno, L., C. D'Aniello, C. Naddeo, V. Vittoria, and S. V. Meille. (2002). Elasticity of the oriented mesomorphic form of syndiotactic polypropylene. *Macromolecules* **35**, 3921–3927.
[72] Sevegney, M. S., G. Parthasarthy, R. M. Kannan, D. W. Thurman, and L. Fernandez-Ballester. (2003). Deformation-induced morphology changes and orientation behavior in syndiotactic polypropylene. *Macromolecules* **36**, 6472–6483.
[73] Parthasarthy, G. (2002). Rheo-optic deformation and crystallization studies on polypropylene. M. S. thesis. Wayne State University.
[74] Hu, Y. R., M. T. Krejchi, C. D. Shah, C. L. Myers, and R. M. Waymouth. (1998). Elastomeric polypropylenes from unbridged (2-phenylindene)zirconocene catalysts: Thermal characterization and mechanical properties. *Macromolecules* **31**, 6908–6916.
[75] Carlson, E. D., M. T. Krejchi, C. D. Shah, T. Terakawa, R. M. Waymouth, and G. G. Fuller. (1998). Rheological and thermal properties of elastomeric polypropylene. *Macromolecules* **31**, 5343–5351.

[76] Kravchenko, R., A. Masood, and R. M. Waymouth. (1997). Propylene polymerization with chiral and achiral unbridged 2-arylindene metallocenes. *Organometallics* **16**, 3635–3639.
[77] Wiyatno, W., G. G. Fuller, J. A. Pople, A. P. Gast, Z. R. Chen, R. M. Waymouth, and C. L. Myers. (2003). Component stress-strain behavior and small-angle neutron scattering investigation of stereoblock elastomeric polypropylene. *Macromolecules* **36**, 1178–1187.
[78] Wiyatno, W., J. A. Pople, A. P. Gast, R. M. Waymouth, and G. G. Fuller. (2002). Dynamic response of stereoblock elastomeric polypropylene studied by rheooptics and X-ray scattering. 1: Influence of isotacticity. *Macromolecules* **35**, 8488–8497.
[79] Wiyatno, W., J. A. Pople, A. P. Gast, R. M. Waymouth, and G. G. Fuller. (2002). Dynamic response of stereoblock elastomeric polypropylene studied by rheooptics and X-ray scattering. 2: Orthogonally oriented crystalline chains. *Macromolecules* **35**, 8498–8508.
[80] Schonherr, H., W. Wiyatno, J. Pople, C. W. Frank, G. G. Fuller, A. P. Gast, and R.M. Waymouth. (2002). Morphology of thermoplastic elastomers: Elastomeric polypropylene. *Macromolecules* **35**, 2654–2666.
[81] No sample is being stretched during calibration, thus further signal processing (at 20 Hz) is unnecessary.
[82] It should also be noted that during open-beam conditions, the lock-in amplifier phase angle is adjusted to provide maximum signal output through a single (“in-phase”) channel.

APPENDIX

Calibration and Background Spectra

Dynamic Phase Calibration

Before collecting any DIRLD data, the spectrometer must be calibrated in order to synchronize the dynamic rheometer with the stepping action of the interferometer mirrors. In this procedure, the dynamic rheometer is used as a chopper (amplitude modulator) to determine the phase lag imposed by the hardware. A small, optically opaque piece of paper is mounted into the oscillating jaw. The dynamic rheometer is then positioned into the path of the IR beam such that approximately one-half of the overall signal intensity is cut off. The software then adjusts the spectrometer phase response for a specific pair of interferometer phase modulation and rheometer stretching frequencies Once this calibration is complete, it needs to be repeated only if any changes in the optical train positioning or modulation parameters are made.

Background Spectra for DIRLD Measurements

In order to convert “raw” processed dynamic signals into quantitative DIRLD spectra, it is necessary to acquire appropriate background spectra. Two different sets of background spectra (obtained without a

sample) must be collected before acquiring spectra of polymer films. Each set consists of two spectra, both obtained with the PEM activated. One set, indicated by a subscript "D," results from performing only one demodulation step at the interferometer phase modulation frequency using the spectrometer DSP electronics[81]. The other set, indicated by a subscript "B," is additionally demodulated by a lock-in amplifier that is referenced to twice the intrinsic PEM frequency. The first pair of background spectra is referred to as the "aligned-polarizer" spectra (P_B and P_D), where a second linear polarizer is placed between the PEM and detector (in place of the usual sample film), providing maximum optical anisotropy. The second polarizer axis is aligned parallel to that of the first polarizer. P_B and P_D contain information about both the polarization modulation efficiency of the PEM and the anisotropy of the optical train. The second pair (M_B and M_D), referred to as the "open-beam" spectra, is obtained with no second polarizer mounted in the IR beam path[82]. M_B and M_D provide information about the optical throughput of the instrument. In summary, four different spectra are obtained in order to normalize dynamic sample spectra.

Background Spectra for Static IRLD Measurements

Similar to dynamic measurements, raw static spectra also need to be normalized appropriately in order to obtain meaningful quantitative results. Static IRLD experiments, however, involve three different pairs of background spectra: aligned-polarizer (P_B and P_D), "crossed-polarizer" (Q_B and Q_D), and open-beam (M_B and M_D). Aligned-polarizer and open-beam spectra are acquired in a manner identical to that used in acquiring DIRLD background spectra. Q_B and Q_D are obtained analogously by rotating the second polarizer (used in acquiring P_B and P_D) 90°. It can be seen from Figure 8 that background spectra typically are not very complex functions of IR wavenumber. In fact, the optical train imposes only a relatively mild dependence of IR absorbance on wavenumber.

Data Acquisition and Analysis

Dynamic Data Acquisition

Using Bio-Rad Win-IR Pro software, DIRLD experiments are performed in step-scan DSP(2) mode, with the spectrometer digital signal processing electronics executing two of three demodulation steps. For the present work, we chose a moving mirror step rate of one per second (1 Hz), a spectral resolution of $8\,cm^{-1}$, and a co-addition of eight scans. Data acquisition requires about two and one-half hours in step-scan DSP(2) mode.

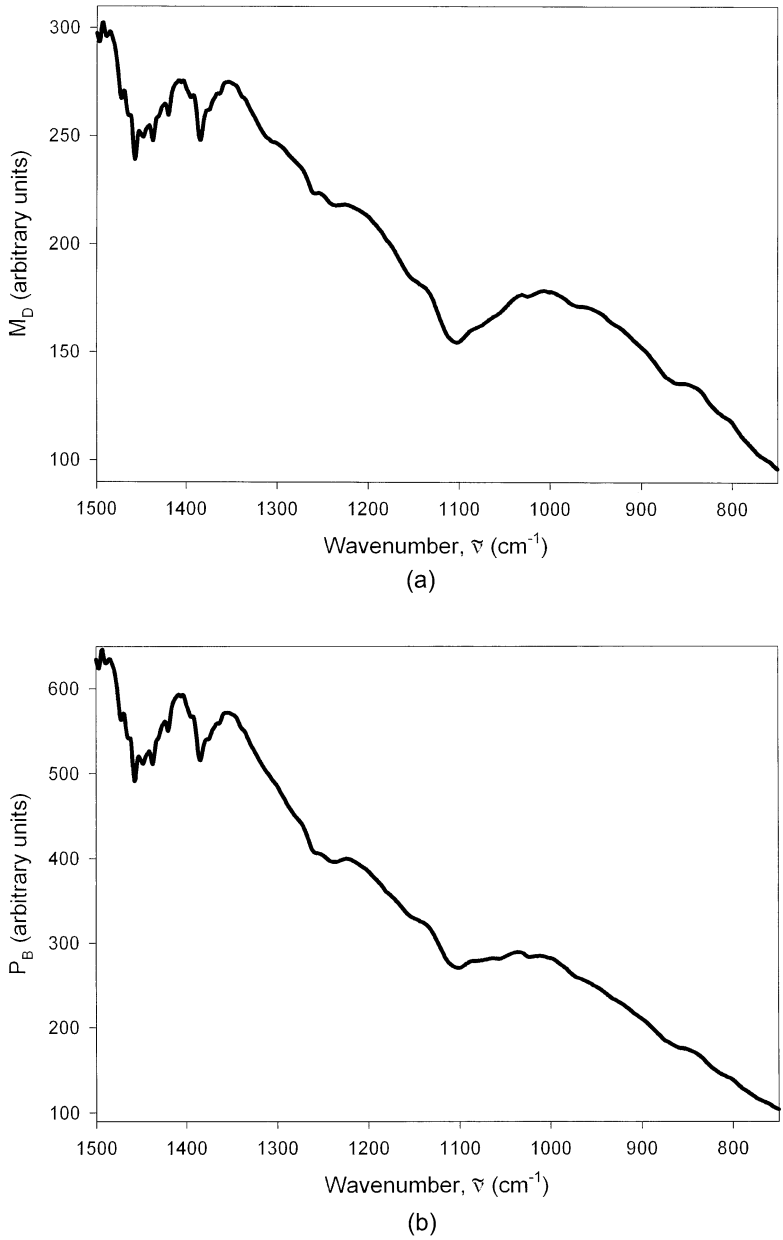

FIGURE 8 Typical background spectra for IRLD experiment, resulting from instrument effects: (a) an "open-beam" absorbance spectrum (M_D); (b) an "aligned-polarizer" dichroism spectrum (P_B).

The IR beam originating from the spectrometer source is intensity modulated by the interferometer in step-scan mode. Unlike continuous-scan FTIR spectroscopy, where the interferometer mirror is moved with constant velocity throughout data acquisition, the mirror is stopped during data collection in step-scan mode. As previously mentioned, however, modulation of the IR beam is still achieved by imposing a dithering (phase modulation) onto the mirror with peak-to-peak modulation amplitude of $2\,\lambda_{\text{He–Ne laser}} \approx 12.7\,\mu\text{m}$. As a result, the time dependence of the interferogram is changed so that no overlapping with other time-dependent phenomena occurs during data acquisition. Thus, sample-related intensity variations can be clearly distinguished from other effects during signal demodulation. It should be recalled that the PEM introduces a second modulation to the IR beam and a third modulation is imposed using the dynamic rheometer. The double-modulated IR beam is focused onto a thin polymer film ($15\,\text{mm} \times 10\,\text{mm} \times \sim 0.03\,\text{mm}$) that is clamped into the micro-rheometer and subjected to a 20 Hz small-amplitude sinusoidal strain. The resulting triple-modulated signal is then recorded, digitized, and amplified by the detector. Finally, the raw electronic signal is passed on to the signal processing train (Figure 9) for demodulation.

The preamplified detected signal is sent along one of two processing paths. The first path involves a high-pass filter, which is used to reject any signal not carried by the high-frequency PEM modulation. A lock-in amplifier (Stanford Research Systems, Model SR830) subsequently demodulates the $\sim 74\,\text{kHz}$ PEM modulation and sends the resulting signal through a single output channel to the spectrometer DSP electronics. The first DSP step deconvolutes the 400 Hz interferometer phase modulation. The resulting spectrum, $\overline{V}_B$, is proportional to the static dichroism of the sample, $\Delta\overline{A}(\tilde{\nu})$. $\overline{V}_B$ may be demodulated further using DSP electronics with quadrature capability. The two spectra resulting from the final 20 Hz demodulation step, V'_C and V''_C, are proportional to

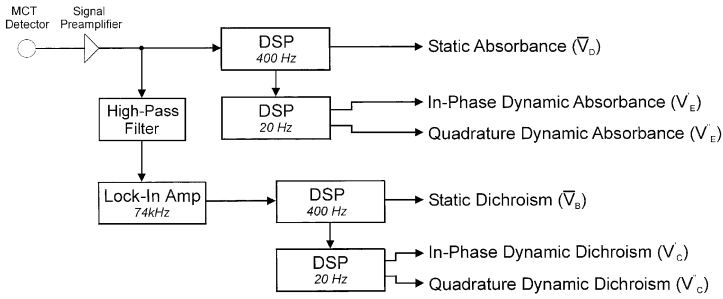

FIGURE 9 Schematic diagram of signal processing/demodulation steps.

the in-phase and quadrature DIRLD spectra ($\Delta A'(\tilde{\nu})$ and $\Delta A''(\tilde{\nu})$), respectively. The second signal path bypasses the lock-in amplifier altogether, sending the signal directly to the spectrometer DSP electronics. The signal resulting from the first (400 Hz) DSP demodulation, $\overline{V}_D$, is proportional to the static absorbance of the sample, $\Delta\overline{A}(\tilde{\nu})$. Further DSP demodulation (at 20 Hz) yields V'_E and V''_E, which are proportional to in-phase and quadrature dynamic absorbances ($A'(\tilde{\nu})$ and $A''(\tilde{\nu})$), respectively. In total, this triple demodulation scheme generates six raw spectra from the detector signal.

Dynamic Data Analysis

The quantitative DIRLD spectra are derived by normalizing raw spectra with appropriate background spectra.[33,46]

$$\Delta A' = \frac{V'_C}{\overline{V}_D}\left(\frac{P_D}{P_B}\right)\left(\frac{M_B}{M_D}\right) \tag{18}$$

$$\Delta A'' = \frac{V''_C}{\overline{V}_D}\left(\frac{P_D}{P_B}\right)\left(\frac{M_B}{M_D}\right) \tag{19}$$

$\Delta A'$ and $\Delta A''$ represent the optical anisotropy of the sample due to dynamic reorientation of individual vibrational moments. $\Delta A'$ represents the extent of instantaneous (or elastic) response to the applied strain, whereas $\Delta A''$ represents the reorientation response that is 90° out of phase (i.e., the "viscous" component). Again, since dichroism spectra are collected directly, it is possible to monitor the response of each moiety simultaneously.

Static Data Acquisition

Static IRLD experiments may be performed in step-scan mode either with or without phase modulation of the moving mirror. A thin polymer film (5 mm × 15 mm × ~0.1 mm) is mounted inside the rheometer using clamps. The rheometer is placed between the PEM and detector with the stretching direction parallel to the axis of the preceding polarizer. Experiments are conducted with a mirror step speed of 400 Hz (i.e., steps per second—no phase modulation) with a resolution of 8 cm^{-1} and 25 scans co-added. Using these parameters, acquisition time is about 30 min; co-addition of four scans requires about 5 min. The polymer film is stretched stepwise at an elongation rate of 0.5 mm/mm while spectra are acquired at each strain point. In contrast to DIRLD measurements, where the IR signal is triply modulated, static experiments involve only a double-modulated IR beam (interferometer and PEM only). Raw dichroism and absorbance spectra ($\overline{V}_B$ and $\overline{V}_D$, respectively) are

computed with the same signal-processing scheme used for DIRLD experiments.

Static Data Analysis

The static IRLD spectrum, $\Delta\overline{A}$, is calculated at each deformation point according to the procedure suggested by Noda et al.[33]. Parallel and perpendicular transmittances are calculated as

$$\overline{T}_{\parallel}(\varepsilon, \nu) = \frac{P_B(\tilde{\nu})\overline{V}_D(\varepsilon, \tilde{\nu}) - P_D(\tilde{\nu})\overline{V}_B(\varepsilon, \tilde{\nu})}{P_B(\tilde{\nu})M_D(\tilde{\nu}) - P_D(\tilde{\nu})M_B(\tilde{\nu})} \tag{20}$$

$$\overline{T}_{\perp}(\varepsilon, \nu) = \frac{Q_B(\tilde{\nu})\overline{V}_D(\varepsilon, \tilde{\nu}) - Q_D(\tilde{\nu})\overline{V}_B(\varepsilon, \tilde{\nu})}{Q_B(\tilde{\nu})M_D(\tilde{\nu}) - Q_D(\tilde{\nu})M_B(\tilde{\nu})} \tag{21}$$

Absorbance is defined as the negative logarithm of transmittance. Thus, static IRLD spectra are expressed as

$$\Delta\overline{A}(\varepsilon, \tilde{\nu}) = -\log\left(\frac{\overline{T}_{\parallel}(\varepsilon, \tilde{\nu})}{\overline{T}_{\perp}(\varepsilon, \tilde{\nu})}\right) \tag{22}$$